2018

Maximizing agility envelopes for reaction wheel spacecraft

Karpenko, Mark; King, Jeffery T.

SAGE

Karpenko, Mark, and Jeffery T. King. "Maximizing agility envelopes for reaction wheel spacecraft." Proceedings of the Institution of Mechanical Engineers, Part G: Journal of Aerospace Engineering (2018).
http://hdl.handle.net/10945/61137

Original Article

Institution of MECHANICAL ENGINEERS
Journal of AEROSPACE ENGINEERING

Proc IMechE Part G:
J Aerospace Engineering
0(0) 1–15

DOI: 10.1177/0954410018787866
journals.sagepub.com/home/pig
SAGE

Maximizing agility envelopes for reaction wheel spacecraft

Mark Karpenko[1] and Jeffery T King[2]

Abstract

Spacecraft agility is limited by the maximum torque that reaction wheels can provide. Therefore, a reaction wheel array is typically configured to maximize the inscribed sphere of the reaction wheel torque envelope. Agility is then determined by dividing the spherical torque by the maximum principal inertia. This industry standard approach can severely underestimate the true capability of an attitude control system. An agility envelope considers the reaction wheel torque envelope along with the spacecraft inertia tensor. The agility envelope can therefore be used as a means to quantify the conservatism associated with the standard approach in order to improve slew performance of a conventional attitude control system without the need for larger, more costly hardware or new control algorithms. This paper, presents a simple approach for constructing the agility envelope of a reaction wheel attitude control system. The agility envelope is applied to determine design curves for limits on angular acceleration and rate for maneuver design and for finding the reaction wheel skew angles that maximize agility for a given spacecraft configuration. A surprising result is the observation that maximizing the inscribed sphere of the reaction wheel torque envelope does not, in general, optimize agility.

Keywords

Spacecraft agility, reaction wheel attitude maneuvering, torque envelope, slew time

Date received: 1 February 2018; accepted: 4 June 2018

Introduction

Attitude maneuvers are typically designed based on kinematics because the resulting spacecraft motion is simple and easy to understand. A rest-to-rest maneuver between any two attitudes, for example, can be completed about a fixed-axis (eigenaxis). This reduces the maneuver synthesis problem to solving the motion of a simple double integrator model. Because the actuators on a real spacecraft have limited performance, in terms of torque and/or momentum, the motion about the eigenaxis will be practically constrained by the maximum acceleration and possibly the maximum angular rate that can be sustained about that axis. For non-rest maneuvers, such as those utilized in a planetary mapping or remote sensing application, the axis of rotation is no longer fixed. However, the same acceleration and rate limits used to design an eigenaxis slew are often applied to non-rest maneuvers. In this case, the slew performance of the spacecraft is limited by the worst-case acceleration and rate limits for any axis. This type of control logic has stood the test of time and is therefore embedded in many practical satellite attitude control systems.[1–5]

When sizing the attitude control system for a new satellite, it is necessary to translate requirements on agility into requirements on the torque and momentum storage capabilities of the actuators. To achieve this mapping, the time to slew through a given angle, Θ, is first related to the eigenaxis acceleration and rate limits using an equation such as

$$t_{\text{slew}} = \sqrt{\frac{4\Theta}{\alpha_{\max}}} \tag{1}$$

for a small angle slew that does not reach a rate limit, and

$$t_{\text{slew}} = \frac{\Theta}{\omega_{\max}} + \frac{\omega_{\max}}{\alpha_{\max}} \tag{2}$$

for large angle slew cases where a rate limit is reached.

[1]Control and Optimization Laboratories, Mechanical and Aerospace Engineering Department, Naval Postgraduate School, Monterey, USA
[2]Department of Aerospace Engineering, United States Naval Academy, Annapolis, USA

Corresponding author:
Jeffery T King, Department of Aerospace Engineering, United States Naval Academy, 590 Holloway Rd, Annapolis, MD 21402, USA.
Email: jking@usna.edu

Once the appropriate acceleration and rate limits are determined from the required slew times, minimum torque and momentum requirements can be defined based on an estimate of the vehicle inertia tensor. This is usually done by finding the largest principal inertia to get

$$\tau_{\text{req}} = I_{\max}\alpha_{\max} \tag{3}$$

and

$$h_{\text{req}} = I_{\max}\omega_{\max} \tag{4}$$

Equations (3) and (4) can also be rearranged, once the attitude control system has been designed, in order to determine the maximum acceleration and rate for maneuver design.

Karpenko et al.[6] demonstrated that equations like (3) and (4) can severely underestimate the capability of the attitude control system. This is because the spacecraft mass properties are generally non-uniform over the sphere whereas equations (3) and (4) assume spherical worst-case mass properties. Consequently, there exist axes of rotation where the effective inertia is much less than $I_{\max}$ leading to the possibility that $\alpha \gg \alpha_{\max}$ and $\omega \gg \omega_{\max}$ for some maneuvers. Moreover, the actuator control space is also generally non-spherical so the axis of maximum torque authority may not be aligned with the principal axes leading to additional conservatism in equations (3) and (4). The conservatism inherent in the standard design equations can therefore 'hide' the true capabilities of the spacecraft attitude control system from the operator.

In an effort to reduce conservatism in design, this paper presents an approach for constructing an agility envelope for reaction wheel attitude control systems. The agility envelope is an extension of the concept of the agilitoid.[7] The agilitoid – a play on the classical inertia ellipsoid[8] – is a three-dimensional visual representation of the maneuverability of a rigid body characterized by the torque-to-inertia ratio about an arbitrary control axis. The agilitoid was developed originally to quantify the 'hidden' agility described above that can be re-claimed through the use of non-standard, off-eigenaxis, maneuvers.[1,9]

In contrast to the agilitoid described in King and Karpenko,[10] the agility envelope describes the true capability of an attitude control system for conventional maneuvering about a given eigenaxis as opposed to off-eigenaxis rotations. In this paper, a simple approach for constructing the agility envelope is presented that allows the correct values $\alpha_{\max}$ and $\omega_{\max}$ for eigenaxis slewing to be computed in a straight forward fashion, for any reaction wheel array. Using the agility envelope, it is also shown that the reaction wheel skew angle that maximizes agility is not necessarily the same as the one that maximizes the inscribed sphere of the reaction wheel torque envelope as implied by previous work.[11,12] Using the concept of the agility envelope, simple design equations are developed for selecting the ideal reaction wheel skew angle to maximize spacecraft agility. Standard three, four, and six wheel configurations are studied. A design example and simulation performance analysis for a notional four reaction wheel spacecraft provides a practical scenario to illustrate the concepts.

Reaction wheel agility envelopes

The reaction wheel torque envelope

In order to describe the construction of the agility envelope for a reaction wheel spacecraft, it is useful to first discuss the capabilities of the reaction wheel system in the torque/momentum space since this is typically the point of view from which agility estimates are derived. An excellent discussion on the geometry of reaction wheel torque and momentum envelopes is given in Markley et al.[12] and this paper makes use of some of these results in the discussion that follows.

Consider two reaction wheels whose spin axes with respect to a body-fixed frame are described by unit-vectors, $\hat{\mathbf{z}}_1 = [\cos(\eta), 0, \sin(\eta)]^T$ and $\hat{\mathbf{z}}_2 = [0, \cos(\eta), \sin(\eta)]^T$, where the parameter η refers to the reaction wheel skew angle. These reaction wheels can produce torque along any vector lying in a plane having the normal $\mathbf{n}_{12} = \hat{\mathbf{z}}_1 \times \hat{\mathbf{z}}_2 = [-\cos(\eta)\sin(\eta), -\cos(\eta)\sin(\eta), \cos^2(\eta)]^T$. Due to the finite torque capacity of the wheels, the magnitude of the torque vector is restricted to lie within a parallelogram, with sides parallel to $\hat{\mathbf{z}}_1$ and $\hat{\mathbf{z}}_2$. As shown in Figure 1(a), the vertices of the parallelogram are obtained when both wheels are saturated at $\pm\tau_{\max}$, and the edges are obtained when either wheel 1 or wheel 2 is unsaturated. (In this paper, as in Markley et al.,[12] all wheels are assumed to be identical in torque and momentum capacities. This is done for simplicity of the exposition. The results, however, hold for the case of non-uniform wheels as well.)

In Figure 1(b), an additional reaction wheel is added with a spin axis along, $\hat{\mathbf{z}}_3 = [0, -\cos(\eta), \sin(\eta)]^T$. The effect of the additional wheel is to translate the '*ij*' parallelogram formed by wheels $i=1$ and $j=2$ by an amount equal to τ_3 along the vector $\hat{\mathbf{z}}_3$. The maximal translation, $\boldsymbol{\delta}_{12} = \tau_{\max}\hat{\mathbf{z}}_3$, occurs when wheel three is saturated, i.e. $\tau_3 = \tau_{\max}$. Moreover, due to inversion symmetry, a second maximal parallelogram is obtained by reversing all of the wheel torques so that the '*ij*' parallelogram is translated by $-\boldsymbol{\delta}_{ij}$ along $\hat{\mathbf{z}}_3$, i.e. $-\boldsymbol{\delta}_{12} = -\tau_{\max}\hat{\mathbf{z}}_3$. These two shifted parallelograms become the end caps of a parallelepiped defined by the vectors, $\hat{\mathbf{z}}_1$, $\hat{\mathbf{z}}_2$, and $\hat{\mathbf{z}}_3$. This parallelepiped describes the volume of the control space that is

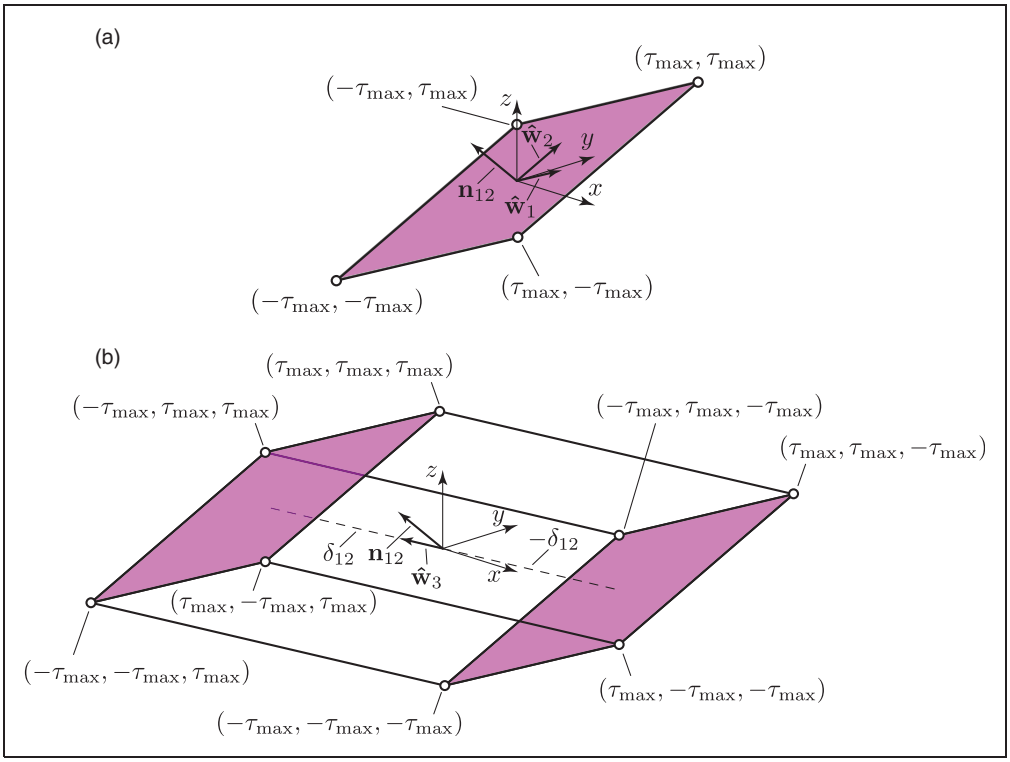

Figure 1. Torque plane for two reaction wheels: (a) bounding parallelogram; (b) control space obtained by adding a third wheel.

achievable using the three reaction wheels. In systems with n wheels, the possible translations, $\boldsymbol{\delta}_{ij}$, of each 'ij' parallelogram are obtained as

$$\boldsymbol{\delta}_{ij} = \tau_{\max} \sum_{k=1,\, k\neq i,j}^{n} \hat{\mathbf{z}}_k \sigma_k \tag{5}$$

where $\sigma = [\sigma_1, \sigma_2, \ldots, \sigma_n]^T$ is an $n \times 1$ vector having elements, $\sigma_i \in \{-1, 1\}$. In other words, the 2^{n-2} translations of each 'ij' torque parallelogram are obtained by adding the various sign permutations of unit-vectors $\hat{\mathbf{z}}_k$ for $k \neq i, j$ and scaling by $\tau_{\max}$.

The reaction wheel torque envelope can be constructed by shifting $n(n-1)/2$ torque parallelograms (one for each 'ij' wheel pair) according to (5) to obtain facets[12] that give the bounding planes of the torque envelope in three-dimensional space. On each facet, all but the i and j wheels are saturated. The reaction wheel torque envelope is simply an extension of the notion of the control parallelepiped defined above for three wheels: the reaction wheel torque envelope is a polyhedron describing the space of the available control torque. Although each 'ij' wheel pair produces 2^{n-2} shifted parallelograms, it is noted in Markley et al.[12] that not all of these will be bounding facets. An example torque envelope for a typical four-wheel attitude control system is shown in Figure 2. For this torque envelope, the reaction wheel alignment matrix, $\mathbf{Z} = [\hat{\mathbf{z}}_1, \hat{\mathbf{z}}_2, \ldots, \hat{\mathbf{z}}_n]^T$, follows a NASA standard four-

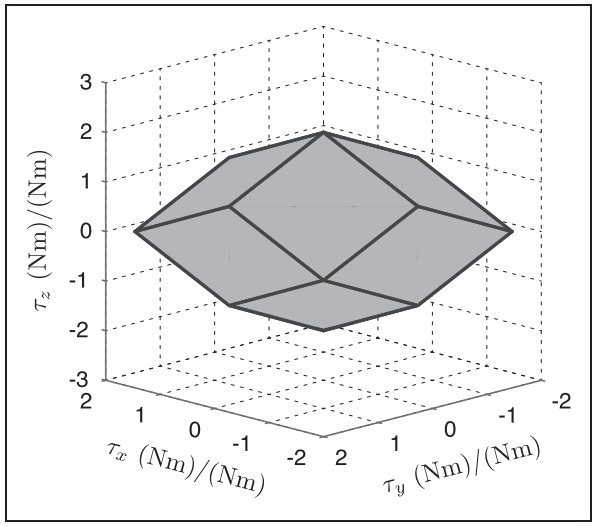

Figure 2. Example reaction wheel torque envelope for a typical four-wheel configuration normalized by $\tau_{\max}$.

wheel configuration[13] and is given as

$$\mathbf{Z} = \begin{bmatrix} \cos(\eta) & 0 & -\cos(\eta) & 0 \\ 0 & \cos(\eta) & 0 & -\cos(\eta) \\ \sin(\eta) & \sin(\eta) & \sin(\eta) & \sin(\eta) \end{bmatrix} \tag{6}$$

with $\eta = 30^\circ$ and the coordinate axes normalized to unity by $\tau_{\max}$. Thus, the normalized torque envelope is the same for any reaction wheel array having the

geometric arrangement given by equation (6). It is also worthwhile to point out that for reaction wheels, the geometry of the momentum envelope is identical to the geometry of the torque envelope. The two differ only in their relative scale and units. Therefore, Figure 2 can alternatively be interpreted as the normalized momentum envelope.

Having described the construction of the reaction wheel torque (or equivalently momentum) envelope, the focus may now be turned to evaluating the size of the largest sphere inscribed within the envelope. This is because in conventional design practice, the spherical torque envelope provides a convenient proxy for agility. The approach presented in Markley et al.[12] for determining the size of the envelope inscribed sphere is based on computing the maximum reaction wheel torque that can be realized in the direction of the normal to each of the '*ij*' facets on the bounding polyhedron. The maximum reaction wheel torque normal to facet '*ij*' is found as the length of a line drawn from the origin, O, to a point, P_{ij}, on facet '*ij*' such that the line $\overline{OP_{ij}}$ is also normal to the '*ij*' facet. An equation for the length, r_{ij}, of line $\overline{OP_{ij}}$ is given by

$$r_{ij} = |\overline{OP_{ij}}| = \tau_{\max} \sum_{k=1}^{n} |\hat{\mathbf{z}}_k \cdot \hat{\mathbf{n}}_{ij}| \tag{7}$$

Note that wheels i and j do not contribute to the sum in equation (7) because these wheels cannot produce a torque along $\hat{\mathbf{n}}_{ij}$. Thus, $\hat{\mathbf{z}}_i \cdot \hat{\mathbf{n}}_{ij} = \hat{\mathbf{z}}_j \cdot \hat{\mathbf{n}}_{ij} = 0$ in equation (7). It is not necessary to distinguish between the '*ij*' facet and the '*ji*' facet because $r_{ij} = r_{ji}$ due to inversion symmetry. Since equation (7) provides the maximum reaction wheel torque normal to any facet, the minimum value of r_{ij} over all the facets gives the radius of the torque envelope inscribed sphere, i.e. $r_\tau = \min_{i,j}\{r_{ij}\}$. This last statement is true even though, for some facets, the line from the origin parallel to $\hat{\mathbf{n}}_{ij}$ may end at a point on the *ij* facet that is not part of the bounding polyhedron. This is because r_{ij} is not, in general, parallel to $\hat{\mathbf{n}}_{ij}$. Interested readers are directed to Markley et al.,[12] which elaborates further on this point.

A conservative agility estimate

To appreciate the utility of the spherical approximation of the reaction wheel torque envelope, consider the well-known equation of motion for a rigid reaction wheel satellite:

$$\mathbf{I}\boldsymbol{\alpha} + \boldsymbol{\omega} \times (\mathbf{I}\boldsymbol{\omega} + \mathbf{Z}\mathbf{h}^w) = -\mathbf{Z}\tau^w \tag{8}$$

where $\boldsymbol{\alpha}$ is the angular acceleration vector, $\mathbf{I}$ is the spacecraft inertia tensor, $\boldsymbol{\omega}$ is the angular rate vector and $\mathbf{Z}$ is the reaction wheel alignment matrix. Vectors $\mathbf{h}^w = [h_1, h_2, \ldots, h_n]^T$ and $\tau^w = [\tau_1, \tau_2, \ldots, \tau_n]^T$ are the reaction wheel momenta and control torques, respectively, defined in the reaction wheel frames.

For a net-zero bias attitude control system the sum, $\mathbf{I}\boldsymbol{\omega} + \mathbf{Z}\mathbf{h}^w = \mathbf{0}$, due to the conservation of angular momentum. Accordingly, equation (8) simplifies to

$$\mathbf{I}\boldsymbol{\alpha} = -\mathbf{Z}\tau^w \tag{9}$$

Moreover, if the torque envelope is approximated as a sphere with radius $r_\tau = \min_{i,j}\{r_{ij}\}$, equation (9) may be further simplified as

$$\mathbf{I}\boldsymbol{\alpha} = -\tau\hat{\mathbf{v}} \tag{10}$$

where τ is the scalar torque magnitude, $0 \leqslant \tau \leqslant r_\tau$, and the arbitrary torque direction is given by unit-vector $\hat{\mathbf{v}}$. For a constant τ, the motion of the satellite will be about the eigenaxis, $\hat{\mathbf{e}}$, so equation (10) may be further manipulated to yield

$$\alpha\hat{\mathbf{e}} = -\tau\mathbf{I}^{-1}\hat{\mathbf{v}} \tag{11}$$

where α is the angular acceleration magnitude about the eigenaxis. Equation (11) emphasizes the fact that the direction of rotation is not the same as the direction of the applied torque, i.e. $\hat{\mathbf{e}} \neq \hat{\mathbf{v}}$, but rather

$$\hat{\mathbf{v}} = \frac{\mathbf{I}\hat{\mathbf{e}}}{||\mathbf{I}\hat{\mathbf{e}}||_2} \tag{12}$$

where notation $||\cdot||_2$ denotes the 2-norm. Thus, the application of equation (11) towards estimating the worst-case (minimax) satellite agility is cumbersome.

However, in the special case of uniform spherical inertia where $\mathbf{I} = I_{\max}[\mathbf{I}]$ with $[\mathbf{I}]$ being the identity matrix, the torque direction and the axis of rotation are parallel, i.e. $\hat{\mathbf{e}} = -\hat{\mathbf{v}}$. In this case, equation (11) may be recast as

$$\alpha\hat{\mathbf{e}} = \frac{\tau}{I_{\max}}\hat{\mathbf{e}} \tag{13}$$

Equation (13) now allows a simple estimate of the maximum angular acceleration, $\alpha_{\max}$, to be obtained by taking the inscribed spherical torque, $\tau = r_\tau$, and the maximum principal moment of inertia as the bounding values. Thus, the agility of the satellite may be estimated as:

$$\alpha_{\max} = \frac{r_\tau}{I_{\max}} \tag{14}$$

The maximum angular rate, $\omega_{\max}$, can be similarly determined by using an analogous equation, $\omega_{\max} = r_h/I_{\max}$, where r_h is the radius of the momentum sphere that has been allocated for slew. Although commonly used for design,[14] equation (14) is deceptive because, in general, neither the inertia tensor nor the torque capability are spherical. Consequently, the

agility of the satellite can be significantly underestimated by using this standard design equation.[6]

Constructing the reaction wheel agility envelope

To more accurately determine the minimax angular acceleration, consider again equation (9), with the assumptions of spherical torque and inertia envelopes purposefully avoided.

$$\boldsymbol{\alpha} = -\mathbf{I}^{-1}\mathbf{Z}\tau^{w} = \mathbf{A}\tau^{w} \tag{15}$$

where the $3 \times n$ matrix $\mathbf{A} = -\mathbf{I}^{-1}\mathbf{Z}$ is called an agility matrix. Similar to the reaction wheel torque distribution matrix, $\mathbf{Z}$, which maps the individual reaction wheel torques to a torque vector in three-dimensional space, the agility matrix $\mathbf{A}$ maps the individual reaction wheel torques to an acceleration vector in three-dimensional space. It includes the negative sign, which ensures the opposite reaction of the spacecraft to the wheel torques. Unlike the reaction wheel torque distribution matrix, the columns, $\mathbf{a}_i$, of the agility matrix, $\mathbf{A} = [\mathbf{a}_1, \mathbf{a}_2, \ldots, \mathbf{a}_n]^T$, are not unit-vectors. Nonetheless, the rigid-body agility equation, $\boldsymbol{\alpha} = \mathbf{A}\tau^{w}$ has precisely the same form as the equation describing the reaction wheel torque mapping. Thus, it appears that an envelope describing the agility of the satellite can be constructed similarly to a reaction wheel torque (or momentum) envelope.

To illustrate the construction of the agility envelope, consider an example satellite having a reaction wheel alignment matrix given by equation (6) and an inertia tensor given as

$$\mathbf{I} = \begin{bmatrix} 42.31 & 0.86 & -3.01 \\ 0.86 & 35.83 & 1.69 \\ -3.01 & 1.69 & 25.86 \end{bmatrix} \text{kg} \cdot \text{m}^2 \tag{16}$$

Similar to the torque plane formed by two reaction wheels, the agility imparted by any two reaction wheels, i and j, also lies in a plane. Accounting for the agility due to a third reaction wheel creates an agility parallelepiped, and for an n-wheel system an agility polyhedron in three-dimensional space. In fact, the vertices of the agility polyhedron are simply the scaled and rotated vertices of the torque polyhedron. To see this, consider the fact that the inertia tensor can be decomposed as

$$\mathbf{I} = \mathbf{V}\boldsymbol{\Lambda}\mathbf{V}^{T} \tag{17}$$

where $\mathbf{V}$ is an orthogonal matrix of eigenvectors and $\boldsymbol{\Lambda}$ is a diagonal matrix of eigenvalues of $\mathbf{I}$. The agility matrix can therefore be re-written as

$$\mathbf{A} = -\mathbf{I}^{-1}\mathbf{Z} = -\mathbf{V}\boldsymbol{\Lambda}\mathbf{V}^{T}\mathbf{Z} \tag{18}$$

From a geometric point of view, the matrix product $\mathbf{V}\boldsymbol{\Lambda}\mathbf{V}^{T}$ represents a series of affine transformations applied to the columns of matrix $\mathbf{Z}$. For example, matrix $\mathbf{V}$ is an affine rotation matrix and diagonal matrix $\boldsymbol{\Lambda}$ is an affine scaling matrix. This transformation has the effect of scaling and rotating each of the original torque parallelograms into agility parallelograms, as shown in Figure 3. As pointed out in Markley et al.,[12] the polyhedron representing the reaction wheel torque envelope is the convex hull of the projection into three-dimensional space of an n-dimensional hypercube in reaction wheel space. Since the composition of a series of affine transformations is also an affine transformation, the agility envelope is also convex, as a convex polyhedron under any affine transformation remains a convex polyhedron.[15,16] In the case of the agility envelope, however, the polyhedron is the convex hull of the projection of the scaled and rotated vertices of the original n-dimensional hypercube. Thus, the agility envelope is a new and important way of extending the work on maximum torque and momentum envelopes described in Markley et al.[12]

For the example satellite under consideration in this section, the transformation matrices associated with the agility matrix are

$$\mathbf{V} = \begin{bmatrix} 0.9829 & -0.0502 & 0.1771 \\ 0.0801 & 0.9829 & -0.1658 \\ -0.1658 & 0.1771 & 0.9701 \end{bmatrix} \tag{19}$$

and

$$\boldsymbol{\Lambda} = \begin{bmatrix} 42.89 & 0 & 0 \\ 0 & 36.09 & 0 \\ 0 & 0 & 25.02 \end{bmatrix} \text{kg} \cdot \text{m}^2 \tag{20}$$

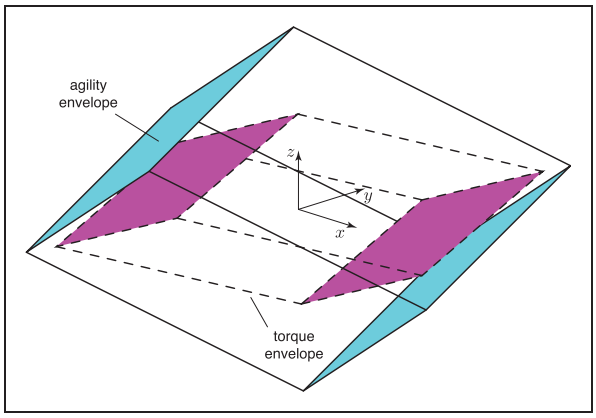

Figure 3. Relative orientations of the torque and agility envelopes for three reaction wheels illustrating the affine transformation of the torque envelope by agility matrix $\mathbf{A} = -\mathbf{I}^{-1}\mathbf{Z}$.

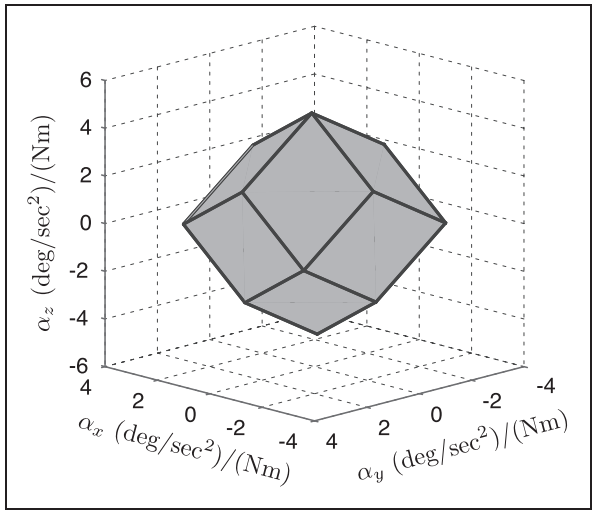

Figure 4. Example agility envelope for a typical four-wheel satellite, normalized by τ_{max}.

The transformation of the torque envelope using (19) and (20) in (18) gives the agility envelope shown in Figure 4. Figure 4 illustrates that the agility envelope is similar, but not identical, to the torque envelope in Figure 2. On the agility envelope, the locations of the vertices for each facet of the torque envelope have been transformed as described above.

For satellite design and maneuver implementation, a better estimate of the angular acceleration and rate capability can be determined by finding largest inscribed sphere within the agility envelope. Since the agility envelope is also a convex polyhedron, equation (7) can be rewritten as

$$r_{\alpha_{ij}} = \tau_{\max} \sum_{k=1}^{n} |-\mathbf{V}\Lambda\mathbf{V}^T\mathbf{z}_k \cdot \hat{\mathbf{n}}_{ij}| = \tau_{\max} \sum_{k=1}^{n} |\mathbf{a}_k \cdot \hat{\mathbf{n}}_{ij}| \tag{21}$$

where the normal vector in (21) should be interpreted as $\mathbf{n}_{ij} = \mathbf{a}_i \times \mathbf{a}_j$ and not $\mathbf{n}_{ij} = \hat{\mathbf{z}}_i \times \hat{\mathbf{z}}_j$ as it was in (7). Using (21), the radius, r_α, of the agility envelope inscribed sphere is simply $r_\alpha = \min_{i,j}\{r_{\alpha_{ij}}\}$. This value represents the actual performance limits of the spacecraft rather than the conservative limits imposed by (14).

Using the agility envelope for evaluating the minimax agility of a reaction wheel satellite, the slew performance can be compared to the agility estimate provided by the standard design equation (14). By evaluating (5) for each wheel pair, it was determined that the reaction wheel torque envelope shown in Figure 2 has an inscribed sphere of radius $r_\tau = 1.55$ (Nm)/(Nm). Therefore, the maximum torque that can be produced in any direction is 1.55 times the torque of an individual wheel. Assume that requirements for a given mission dictate minimum slew acceleration and rate capabilities of 0.4 deg/sec^2 and 3.0 deg/sec, respectively. Using (14) with $I_{\max} = 42.89\,\mathrm{kg}\cdot\mathrm{m}^2$ from (16), the required torque per wheel is $\tau_{\max} \geqslant 0.19$ Nm and the required momentum per wheel is $h_{\max} \geqslant 1.45$ Nms. If the reaction wheels are sized to meet these requirements, e.g. $\tau_{\max} = 0.2$ Nm and $h_{\max} = 1.5$ Nms, the design values of $\alpha_{\max} = 0.4$ deg/sec and $\omega_{\max} = 3.0$ deg/sec^2 may be used as part of a quaternion error feedback system in the form of slew rate and control constraints.[17]

The radius of the inscribed sphere for the agility envelope of Figure 4, is $r_\alpha = 2.33$ (deg/sec^2)/(Nm), which is obtained by evaluating (21) over all the facets. Thus, using the same wheels as dictated by design equation (14), the maximum acceleration and rate that are achievable in any direction are $\alpha_{\max} = \tau_{\max} r_\alpha = 0.2(2.33) = 0.46$ deg/sec^2 and $\omega_{\max} = h_{\max} r_\alpha = 1.5(2.33) = 3.49$ deg/sec. The maneuver rate and acceleration limits (obtained from the analysis of the agility envelope) are approximately 12 percent larger than the conventional analysis (based on the torque envelope). Figure 5 illustrates this by showing that the radius of the acceleration sphere described by equation (14) lies entirely within the agility polyhedron. The difference between the two spheres is a result of the conservatism inherent to equation (14). Figure 5 also shows the cross-section of the agility envelope in the plane containing the 'slow' and 'fast' axes. In Figure 5, the 'slow' axis represents the direction of spacecraft rotation in which the inscribed sphere of the agility envelope touches the bounding facets of the agility polyhedron. Thus, the 'slow' axis represents the minimax agility that can be achieved for a maneuver in any direction. The 'fast' axis, on the other hand, represents the maneuver axis about which the maximum possible agility can be generated, i.e. the direction in which the boundary of the agility polyhedron is farthest from the origin. It can be seen that agility about the 'fast' axis can be much larger than the spherical minimax agility. However, the 'fast' agility can only be realized for maneuvers about the 'fast' axis.

If the standard design equation is used to size the attitude control system, the reaction wheel capabilities may be over-designed and the agility of the attitude control system would be underutilized. The lost performance can be regained, even for on-orbit spacecraft, simply by updating the flight software with the new values of $\omega_{\max}$ and $\alpha_{\max}$ obtained from the agility envelope. Alternatively, by utilizing the agility envelope to initially size the attitude control hardware, 14 percent smaller reaction wheels could be implemented to meet the 0.4 deg/sec and 3.0 deg/sec^2 mission slew requirements. This example demonstrates how the idea of the agility envelope can be used for actuator sizing and/or control system implementation in order to reduce the simplistic estimates associated with standard design equations. The potential for an immediate and essentially free agility improvement for on-orbit assets was a prime motivation for this work. The remainder of this paper explores the geometry of the agility envelope and shows how it can be exploited to

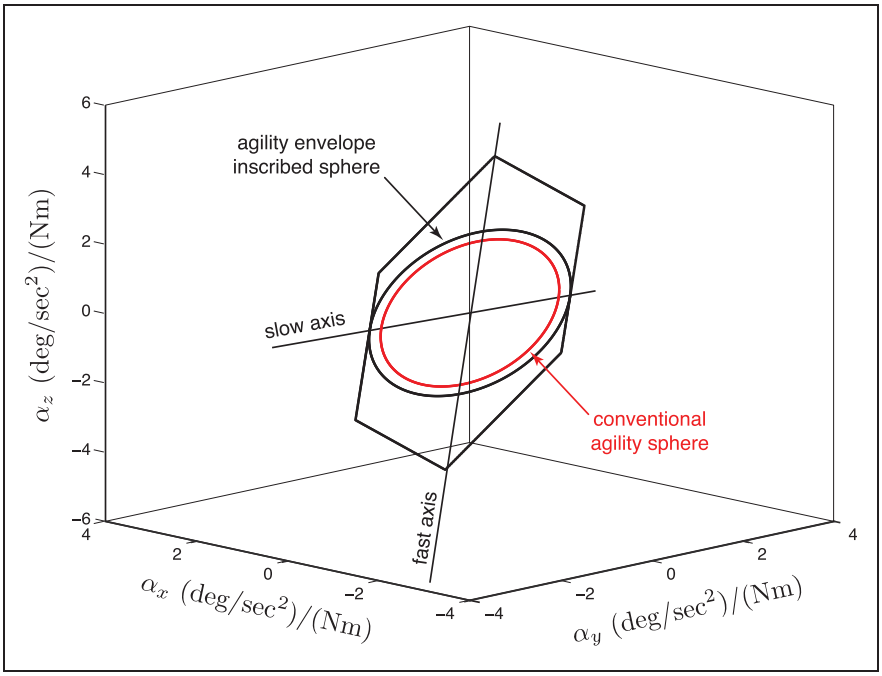

Figure 5. Section of the agility envelope showing the true agility sphere and the smaller-diameter sphere that is obtained when using the conventional analysis.

determine the ideal reaction wheel configuration for a given satellite early in the design of an attitude control system.

Maximizing spherical agility

This section utilizes the new concept of the agility envelope to develop analytical equations for finding ideal reaction-wheel skew angles to maximize agility. These equations, along with the corresponding design curves, can be used in lieu of the conventional design equations for sizing new attitude control systems in order to minimize design conservatism. Results for several NASA standard reaction wheel configurations are presented to illustrate the approach which can be further applied, by interested readers, to maximize the slew performance of other reaction wheel configurations. In this section, it is assumed that the max-norm algorithm of Markley et al.[12] is employed for control allocation. The analysis can, of course, also be performed for control allocation schemes based on the pseudoinverse or other allocation schemes.

Consider, without loss of generality, a generic rigid-body satellite whose mass properties are given by the following inertia tensor

$$\mathbf{I} = I_{xx}\begin{bmatrix} 1 & 0 & 0 \\ 0 & F & 0 \\ 0 & 0 & G \end{bmatrix} \tag{22}$$

where F and G are the ratios of the principal inertia values to I_{xx}, i.e. $F = I_{yy}/I_{xx}$ and $G = I_{zz}/I_{xx}$. Considering the properties of the inertia tensor, there are physical limits to the values that ratios F and G can take, based on the triangle inequalities

$$\frac{|F-G|}{1} < 1 \quad \text{and} \quad \frac{|1-F|}{G} < 1 \quad \text{and} \quad \frac{|1-G|}{F} < 1 \tag{23}$$

Values for F and G that violate (23) are not physically realizable and should not be considered for design analysis.

To further develop the notion of a normalized agility envelope, the agility matrix, $\mathbf{A}$, is redefined as an inertia-normalized agility matrix or

$$\bar{\mathbf{A}} = -\begin{bmatrix} 1 & 0 & 0 \\ 0 & F & 0 \\ 0 & 0 & G \end{bmatrix}^{-1} \mathbf{Z} \tag{24}$$

Consequently, similar to equation (5)

$$\boldsymbol{\alpha} = \frac{\tau_{\max}}{I_{xx}}\,\bar{\mathbf{A}}\bar{\boldsymbol{\tau}}^{w} \tag{25}$$

where $\bar{\boldsymbol{\tau}}^{w}$ is the torque vector in the reaction wheel frame normalized by $\tau_{\max}$. If one defines the radius of the largest inscribed sphere within the normalized agility envelope as $r_{AIS} = \mathcal{A}$, then (25) simplifies to

$$\alpha_{AIS} = \frac{\tau_{\max}}{I_{xx}}\,\mathcal{A} \tag{26}$$

The remainder of this section develops equations for finding the ideal skew angle of three, four, and six

reaction wheel arrays. The ideal skew angle is defined as the one that maximizes the radius of the spherical acceleration envelope, $\mathcal{A}$, for a given satellite configuration.

Ideal skew angle for a three-wheel array

The reaction wheel alignment matrix for a standard NASA three-wheel array[13] is given as

$$\mathbf{Z} = \begin{bmatrix} \cos(\eta) & -\frac{1}{2}\cos(\eta) & -\frac{1}{2}\cos(\eta) \\ 0 & \frac{\sqrt{3}}{2}\cos(\eta) & -\frac{\sqrt{3}}{2}\cos(\eta) \\ \sin(\eta) & \sin(\eta) & \sin(\eta) \end{bmatrix} \tag{27}$$

The inertia-normalized agility matrix is therefore

$$\bar{\mathbf{A}} = -\begin{bmatrix} \cos(\eta) & -\frac{\cos(\eta)}{2} & -\frac{\cos(\eta)}{2} \\ 0 & \frac{\sqrt{3}\cos(\eta)}{2F} & \frac{\sqrt{3}\cos(\eta)}{2F} \\ \frac{\sin(\eta)}{G} & \frac{\sin(\eta)}{G} & \frac{\sin(\eta)}{G} \end{bmatrix} \tag{28}$$

To determine the agility envelope inscribed sphere, equation (21) must be evaluated over all the agility facets. For example, the radius of the sphere touching the '12' agility facet is

$$\mathcal{A}_{12} = \frac{3sc}{\sqrt{s^2 + 3s^2F^2 + c^2G^2}} \tag{29}$$

where $c = \cos(\eta)$ and $s = \sin(\eta)$.

For a diagonal inertia tensor, only three of the six possible facets for a three wheel system need to be considered for evaluation of the agility sphere (due to the inversion symmetry). Moreover, for the wheel configuration of (27), the radial distance from the origin along $\hat{\mathbf{n}}_{ij}$ is the same for two of the three facets. That is, $\mathcal{A}_{12} = \mathcal{A}_{13}$. The equation for the remaining facet is

$$\mathcal{A}_{23} = \frac{3sc}{\sqrt{4s^2 + c^2G^2}} \tag{30}$$

Using (29) and (30), the radius of the inscribed agility sphere is $\mathcal{A} = \min\{\mathcal{A}_{12}, \mathcal{A}_{23}\}$.

In order to maximize the value of $\mathcal{A}$, the following equation must be solved for each agility facet

$$\frac{d\mathcal{A}_{ij}}{d\eta} = 0 \tag{31}$$

Solving (31) gives the ideal value of the skew angle, η_{opt}.

For the '12' and '13' facets, the solution of (31) yields

$$\eta_{opt} = \sin^{-1}\left(\sqrt{\frac{G}{G + \sqrt{1 + 3F^2}}}\right) \tag{32}$$

for which

$$\mathcal{A}_{12}(F, G) = \mathcal{A}_{13}(F, G) = \frac{3}{G + \sqrt{1 + 3F^2}} \tag{33}$$

and for the '23' facet

$$\eta_{opt} = \sin^{-1}\left(\sqrt{\frac{G}{G + 2}}\right) \tag{34}$$

which results in

$$\mathcal{A}_{23}(F, G) = \frac{3}{G + 2} \tag{35}$$

Since the denominator of (33) is larger than the denominator of (35) for $F > 1$, the ideal skew angle for the three-wheel system as a function of F and G is

$$\eta_{opt} = \begin{cases} \sin^{-1}\left(\sqrt{\frac{G}{G+2}}\right) & \text{for } F \leqslant 1 \\ \sin^{-1}\left(\sqrt{\frac{G}{G+\sqrt{1+3F^2}}}\right) & \text{for } F > 1 \end{cases} \tag{36}$$

Using (36), the radius of the agility envelope inscribed sphere for the three-wheel system becomes

$$\mathcal{A}(F, G) = \begin{cases} \frac{3}{G+2} & \text{for } F \leqslant 1 \\ \frac{3}{G+\sqrt{1+3F^2}} & \text{for } F > 1 \end{cases} \tag{37}$$

From the relationships above, generic curves can be plotted for use in design analysis and trade studies. Example design curves for various values of inertia ratios, F and G, are given in Figure 6. The curves adhere to the triangle inequalities of (23).

Ideal skew angle for a four-wheel array

The analysis is now applied to a four reaction wheel system with generic inertia matrix (22). The reaction wheel alignment matrix for a standard four-wheel configuration is specified as:

$$\mathbf{Z} = \begin{bmatrix} c & 0 & -c & 0 \\ 0 & c & 0 & -c \\ s & s & s & s \end{bmatrix} \tag{38}$$

Following the same process as in the previous subsection for finding $\mathcal{A}_{ij}$ in terms of s, c, F, and G yields:

$$\mathcal{A}_{12} = \frac{4sc}{\sqrt{s^2(1 + F^2) + c^2G^2}} \tag{39}$$

$$\mathcal{A}_{13} = \frac{2c}{F} \tag{40}$$

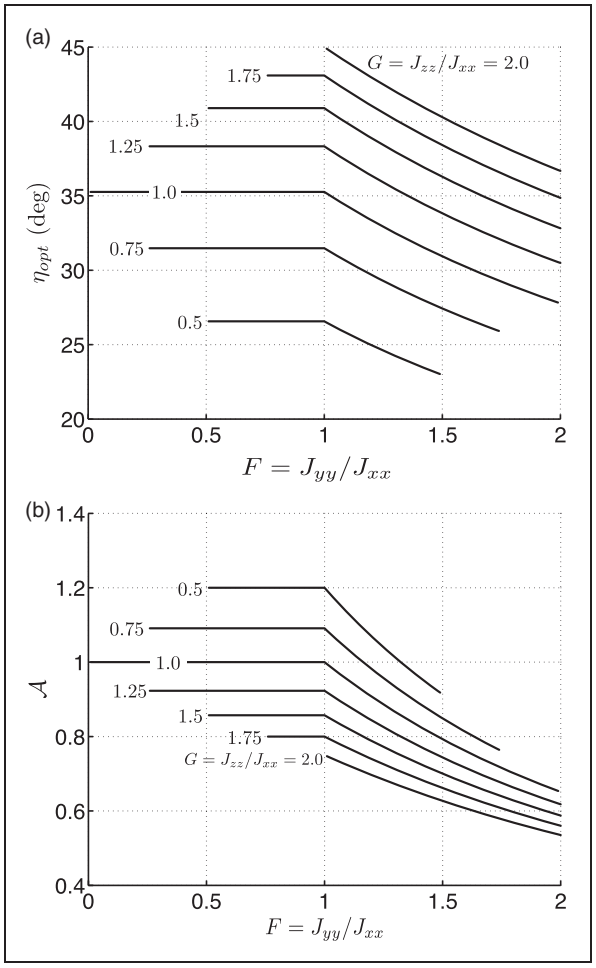

Figure 6. Maximum agility design curves for a NASA standard three-wheel system: (a) optimal skew angle, η_{opt}; (b) normalized radius of agility envelope inscribed sphere, $\mathcal{A}$.

$$\mathcal{A}_{24} = 2c \tag{41}$$

For the four-wheel system with a diagonal inertia tensor, $\mathcal{A}_{ij}$ for the remaining agility facets will be the same as one of (39), (40), or (41). For a symmetric inertia matrix ($F = G = 1$), the expression for the agility sphere simplifies to the conventional one with the radius of the torque sphere provided in Markley et al.[12]

For a non-symmetric inertia tensor, all three unique facets, $\mathcal{A}_{12}, \mathcal{A}_{13}, \mathcal{A}_{24}$, must be considered when maximizing the radius of the spherical acceleration envelope. When $F < 1$, $\mathcal{A}_{24}$ will always be smaller than $\mathcal{A}_{13}$. However, if $F > 1$, then $\mathcal{A}_{13}$ will always be smaller than $\mathcal{A}_{24}$. If $F = 1$, $\mathcal{A}_{24} = \mathcal{A}_{13}$ so both '24' and '13' may be limiting facets.

Finding the solution for the largest spherical acceleration envelope with $F \leqslant 1$ is dependent on the value of ratio G and the relationship between $\mathcal{A}_{12}$ and $\mathcal{A}_{24}$. Specifically, a transition between limiting facets occurs at

$$G = \frac{3 - F^2}{\sqrt{F^2 + 1}} \tag{42}$$

Therefore, the largest acceleration sphere for $G \leqslant (3 - F^2)/\sqrt{F^2 + 1}$ is obtained for the following skew angle

$$\eta_{opt} = \sin^{-1}\left(\frac{G}{\sqrt{3 - F^2 + G^2}}\right) \quad F \leqslant 1, \quad G \leqslant \frac{3 - F^2}{\sqrt{F^2 + 1}} \tag{43}$$

which maximizes $\mathcal{A}$ as

$$\mathcal{A}(F, G) = \frac{2\sqrt{3 - F^2}}{\sqrt{3 - F^2 + G^2}} \quad F \leqslant 1, \quad G \leqslant \frac{3 - F^2}{\sqrt{F^2 + 1}} \tag{44}$$

For values of $G > (3 - F^2)/\sqrt{F^2 + 1}$, the optimal skew angle is

$$\eta_{opt} = \sin^{-1}\left(\sqrt{\frac{G}{G + \sqrt{1 + F^2}}}\right) \quad F \leqslant 1, \quad G > \frac{3 - F^2}{\sqrt{F^2 + 1}} \tag{45}$$

which gives

$$\mathcal{A}(F, G) = \frac{4}{G + \sqrt{1 + F^2}} \quad F \leqslant 1, \quad G > \frac{3 - F^2}{\sqrt{F^2 + 1}} \tag{46}$$

The solution for the largest spherical envelope with $F > 1$ is based on the relationship between $\mathcal{A}_{12}$ and $\mathcal{A}_{13}$, with a transition occurring at

$$G = \frac{3F^2 - 1}{\sqrt{F^2 + 1}} \tag{47}$$

For values of $G \leqslant (3F^2 - 1)/\sqrt{F^2 + 1}$, the ideal skew angle and the maximum value of $\mathcal{A}$ are given by

$$\eta_{opt} = \sin^{-1}\left(\frac{G}{\sqrt{G^2 + 3F^2 - 1}}\right) \quad F > 1, \quad G \leqslant \frac{3F^2 - 1}{\sqrt{F^2 + 1}} \tag{48}$$

$$\mathcal{A}(F, G) = \frac{2\sqrt{3F^2 - 1}}{F\sqrt{G^2 + 3F^2 - 1}} \quad F > 1, \quad G \leqslant \frac{3F^2 - 1}{\sqrt{F^2 + 1}} \tag{49}$$

However, for $G > (3F^2 - 1)/\sqrt{F^2 + 1}$, the optimal skew angle and value of $\mathcal{A}$ are given by (45) and (46), respectively, as these facets become the most restrictive.

Similar to the three-wheel configuration, a set of design curves can be created for the four-wheel system as seen in Figure 7. These curves can be used to quickly determine the parameters of a four-wheel configuration that provides the greatest agility for slewing.

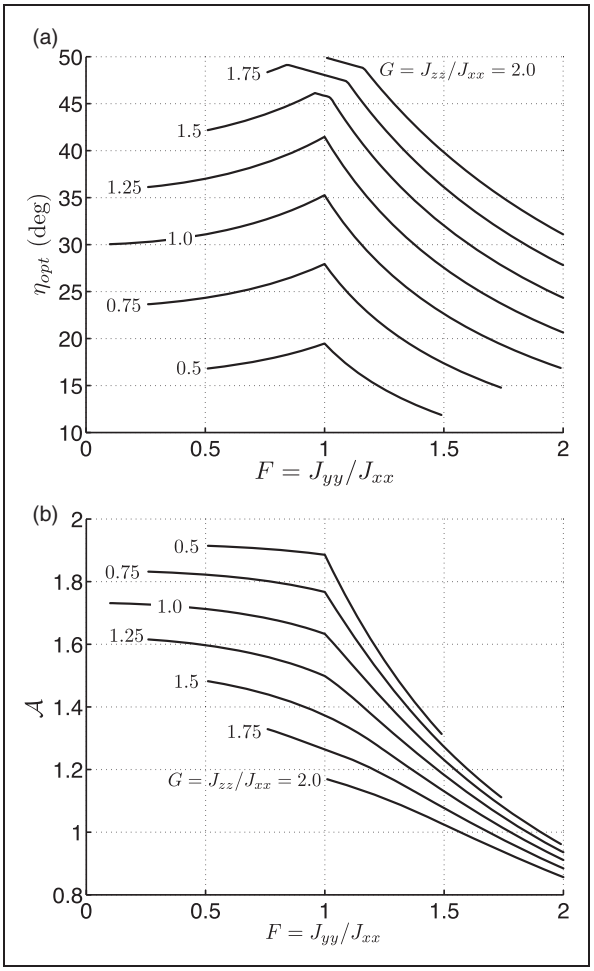

Figure 7. Maximum agility design curves for a NASA standard four-wheel system: (a) optimal skew angle, η_{opt}; (b) normalized radius of agility envelope inscribed sphere, $\mathcal{A}$.

Ideal skew angle for a six-wheel array

For the six reaction wheel system configuration, the NASA standard configuration[13] is:

$$\mathbf{Z} = \begin{bmatrix} c & c/2 & -c/2 & -c & -c/2 & c/2 \\ 0 & \sqrt{3}c/2 & \sqrt{3}c/2 & 0 & -\sqrt{3}c/2 & -\sqrt{3}c/2 \\ s & s & s & s & s & s \end{bmatrix} \tag{50}$$

The unique expressions for each of the 30 possible $\mathcal{A}_{ij}$ are:

$$\mathcal{A}_{12} = \frac{6\sqrt{3}sc}{\sqrt{s^2(3+F^2-3G^2)+3G^2}} \tag{51}$$

$$\mathcal{A}_{13} = \frac{8sc}{\sqrt{s^2(1+3F^2-G^2)+G^2}} \tag{52}$$

$$\mathcal{A}_{14} = \frac{2\sqrt{3}c}{F} \tag{53}$$

Table 1. Ideal skew angle and agility sphere for a non-symmetric spacecraft with six reaction wheels configured per (50) with $F < 1$.

$G \geqslant$	$\sin(\eta_{opt})$	$\mathcal{A}(F,G)$
0	$\frac{\sqrt{3}G}{\sqrt{4F^2+3G^2}}$	$\frac{8\sqrt{3}F}{\sqrt{(3+F^2)(4F^2+3G^2)}}$
$\frac{2F^2}{3}$	$\sqrt{\frac{G}{G+2}}$	$\frac{8}{2+G}$
$\frac{(15-4F^2)(F^2+15+\sqrt{F^4+18F^2+189})}{21(F^2+3)}$	$\frac{\sqrt{21}G}{\sqrt{21G^2-16F^2+60}}$	$\frac{4\sqrt{21(15-4F^2)}}{\sqrt{(9-F^2)(21G^2-16F^2+60)}}$
$\frac{4(15-4F^2)}{7\sqrt{3F^2+9}}$	$\sqrt{\frac{\sqrt{3}G}{\sqrt{3}t+\sqrt{F^2+3}}}$	$\frac{6\sqrt{3}}{\sqrt{3}G+\sqrt{F^2+3}}$

$$\mathcal{A}_{23} = \frac{6\sqrt{3}sc}{\sqrt{s^2(4F^2-3G^2)+3G^2}} \tag{54}$$

$$\mathcal{A}_{25} = \frac{4\sqrt{3}c}{\sqrt{(3+F^2)}} \tag{55}$$

$$\mathcal{A}_{26} = \frac{8sc}{\sqrt{s^2(4-G^2)+G^2}} \tag{56}$$

The remaining agility facets will have expressions the same as one of the facets given in equations (51) to (56).

With a non-symmetric inertia, six of the 30 facets are unique. However, there is an inherent symmetry in the six unique facets that allows them to be further grouped into two sets of three. Similar to the four-wheel scenario, it is the value of F that determines which set of three to use, and it is the values of both F and G that determine the limiting facet or pair of facets within each subset. When $F \leqslant 1$, the limiting facet will be one of $\{\mathcal{A}_{12}, \mathcal{A}_{26}, \mathcal{A}_{25}\}$. When $F \geqslant 1$, the limiting facet will be one of $\{\mathcal{A}_{13}, \mathcal{A}_{14}, \mathcal{A}_{23}\}$. In order to find the largest spherical radius for each combination of F and G, individual relationships between the limiting facets must be understood and quantified. In some cases, one of the three facets is the single limiting facet, but in other cases, two facets are equally constraining and limit the radius of the agility sphere as a pair. There are three distinct regions of F that must be addressed. Tables 1 to 3 give the optimal skew angle, η_{opt}, and the maximum spherical radius, $\mathcal{A}$, in terms of F and G for each region of F. Figure 8 shows the design curves for optimizing the spherical agility envelope for a given spacecraft inertia tensor and a standard six-wheel configuration.

The achievable agility of reaction wheel systems

The benefit of using the agility envelope to define the acceleration limits for a spacecraft is evident by the increased slew performance as compared to the conventional approach. To further elucidate the differences, two possible scenarios are explored for attitude control system design and operation in this section. In the first, it is assumed that the reaction wheel arrays are configured using the conventional

Table 2. Ideal skew angle and agility sphere for a non-symmetric spacecraft with six reaction wheels configured per (50) with $1 \leqslant F \leqslant \sqrt{3/2}$.

$G \geqslant$	$\sin(\eta_{opt})$	$\mathcal{A}(F,G)$
0	$\frac{\sqrt{3}G}{\sqrt{7F^2+3G^2-3}}$	$\frac{2\sqrt{21F^2-9}}{F\sqrt{7F^2+3G^2-3}}$
$\frac{7F^2-3}{3\sqrt{3F^2+1}}$	$\sqrt{\frac{G}{G+\sqrt{3F^2+1}}}$	$\frac{8}{G+\sqrt{3F^2+1}}$
$\frac{17F^2+27}{21\sqrt{3F^2+1}}$	$\frac{\sqrt{21}G}{\sqrt{21G^2+17F^2+27}}$	$\frac{2\sqrt{21(17F^2+27)}}{\sqrt{(21G^2+17F^2+27)(5F^2+3)}}$
$\frac{17F^2+27}{14\sqrt{3}F}$	$\sqrt{\frac{\sqrt{3}G}{\sqrt{3}t+2F}}$	$\frac{6\sqrt{3}}{\sqrt{3}G+2F}$

Table 3. Ideal skew angle and agility sphere for a non-symmetric spacecraft with six reaction wheels configured per (50) with $F > \sqrt{3/2}$.

$G \geqslant$	$\sin(\eta_{opt})$	$\mathcal{A}(F,G)$
0	$\frac{\sqrt{3}G}{\sqrt{3G^2+5F^2}}$	$\frac{2\sqrt{15}}{\sqrt{3G^2+5F^2}}$
$\frac{5\sqrt{3}}{6F}$	$\sqrt{\frac{\sqrt{3}G}{\sqrt{3}G+2F}}$	$\frac{6\sqrt{3}}{\sqrt{3}+2F}$

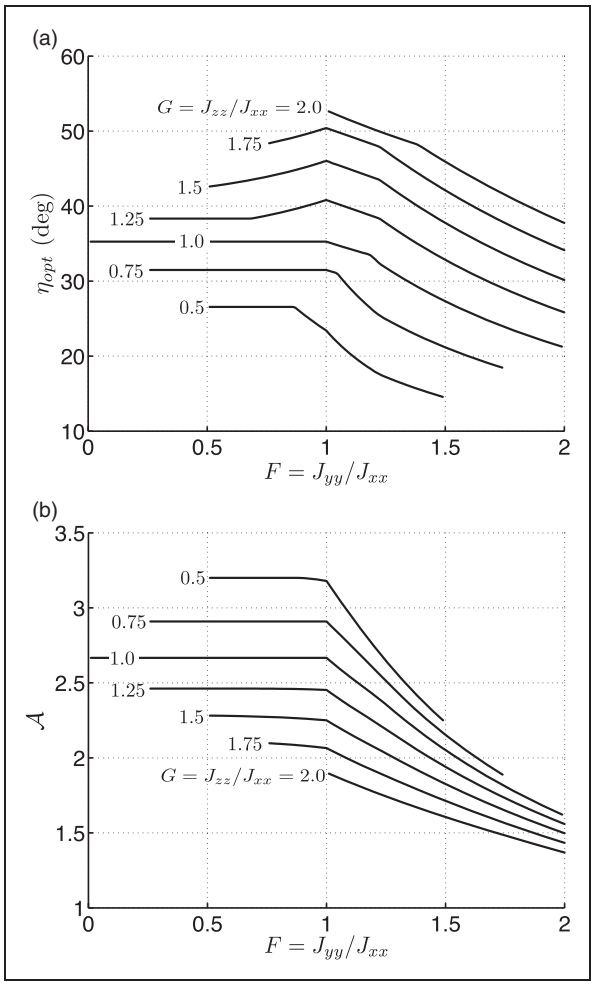

Figure 8. Maximum agility design curves for a NASA standard six-wheel system: (a) optimal skew angle, η_{opt}; (b) normalized radius of agility envelope inscribed sphere, $\mathcal{A}$.

Table 4. Normalized agility estimates for a three-wheel configuration with $\eta = 35.26^\circ$.

(F, G)	$\bar{\alpha}_{\max}$	$\bar{r}_\alpha$	Gain (%)
(1.0, 1.0)	1.00	1.00	–
(1.0, 0.5)	1.00	1.15	15
(1.0, 1.5)	0.67	0.84	25
(0.5, 0.5)	1.00	1.15	15
(0.5, 1.0)	1.00	1.00	–
(0.5, 1.5)	0.67	0.84	25
(1.5, 0.5)	0.67	0.85	27
(1.5, 1.0)	0.67	0.78	16
(1.5, 1.5)	0.67	0.70	4

approach which maximizes the spherical torque/momentum envelopes. This is accomplished when $\eta = 35.26^\circ$, as described in Markley et al.,[12] for the three, four and six-wheel arrays discussed in the last section. Using these reaction wheel configurations the satellite agility limits are solved using the spherical torque/momentum envelopes divided by the largest principal inertia, equation (14), to obtain a normalized sphere having radius, $\bar{\alpha}_{\max}$. The same skew angle, $\eta = 35.26^\circ$ is then used to construct the agility envelope to determine the normalized slew capability, $\bar{r}_\alpha$, from the resulting spherical acceleration envelope and the change in predicted agility is assessed. Tables 4–6 compare the results of the conventional analysis with those obtained by recomputing the slew capability using the agility envelope for the same reaction wheel skew angle across various inertia ratios.

In the second scenario, the change in performance is determined by using the agility envelope to determine the ideal skew angle. In this case, the value of $\mathcal{A}$ is used to define the agility limits for the satellite. Tables 7–9 compare the slew capability obtained by applying the conventional design equations against the slew capability of a reaction wheel array specifically configured to maximize, $\mathcal{A}$, the radius of the agility inscribed sphere. From these latter tables, it is evident that the skew angle that maximizes the spherical torque envelope is not, in general, the same as the skew angle that maximizes agility. In order to translate the data provided in Tables 4 to 9 to a direct acceleration or rate magnitude, it is necessary to multiply the normalized values by $\tau_{\max}$ or $h_{\max}$ and divide the result by I_{xx}, similar to (25), for a given system.

Referring to Tables 4 to 9, it is evident that using the torque or momentum envelope to determine the ideal skew angle for the reaction wheel configuration can underestimate the slew performance of a non-symmetric spacecraft. To further illustrate this severity of this point, Figure 9 shows a contour map of the percent gain in agility for the standard four-wheel configuration studied earlier over a span of inertia ratios, F and G. The performance enhancement is

Table 5. Normalized agility estimates for a four-wheel configuration with $\eta = 35.26^\circ$.

(F, G)	$\bar{\alpha}_{\max}$	$\bar{r}_\alpha$	Gain (%)
(1.0, 1.0)	1.63	1.63	–
(1.0, 0.5)	1.63	1.63	–
(1.0, 1.5)	1.09	1.28	17
(0.5, 0.5)	1.63	1.63	–
(0.5, 1.0)	1.63	1.63	–
(0.5, 1.5)	1.09	1.36	25
(1.5, 0.5)	1.09	1.09	–
(1.5, 1.0)	1.09	1.09	–
(1.5, 1.5)	1.09	1.09	–

Table 6. Normalized agility estimates for a six-wheel configuration with $\eta = 35.26^\circ$.

(F, G)	$\bar{\alpha}_{\max}$	r_α	Gain (%)
(1.0, 1.0)	2.67	2.67	–
(1.0, 0.5)	2.67	2.83	6
(1.0, 1.5)	1.78	2.03	14
(0.5, 0.5)	2.67	3.08	15
(0.5, 1.0)	2.67	2.67	–
(0.5, 1.5)	1.78	2.07	16
(1.5, 0.5)	1.78	1.89	6
(1.5, 1.0)	1.78	1.89	6
(1.5, 1.5)	1.78	1.79	1

Table 7. Maximum spherical agility (normalized) for a three-wheel configuration with η_{opt}.

(F, G)	$\bar{\alpha}_{\max}$	$\mathcal{A}$	η_{opt} (deg)	Gain (%)
(1.0, 1.0)	1.00	1.00	35.26	–
(1.0, 0.5)	1.00	1.20	26.57	20
(1.0, 1.5)	0.67	0.86	40.89	28
(0.5, 0.5)	1.00	1.20	26.57	20
(0.5, 1.0)	1.00	1.00	35.26	–
(0.5, 1.5)	0.67	0.86	40.89	28
(1.5, 0.5)	0.67	0.91	22.97	36
(1.5, 1.0)	0.67	0.79	30.94	18
(1.5, 1.5)	0.67	0.70	36.28	4

obtained by finding the skew angle that maximizes the agility sphere and configuring the reaction wheel array using this value instead of the value obtained by maximizing the torque sphere. The precise value of the performance benefit is dependent on the specific reaction wheel configuration as well as the spacecraft inertia ratios. For the range of F and G values presented here, the performance gain obtained by optimizing the skew angle to maximize $\mathcal{A}$ can be more than 40 percent. This is similarly true for the three, four, and six-wheel arrays and emphasizes the utility of the agility envelope for configuring an agile attitude control system.

Table 8. Maximum spherical agility (normalized) for a four-wheel configuration with η_{opt}.

(F, G)	$\bar{\alpha}_{\max}$	$\mathcal{A}$	η_{opt} (deg)	Gain (%)
(1.0, 1.0)	1.63	1.63	35.26	–
(1.0, 0.5)	1.63	1.89	19.47	16
(1.0, 1.5)	1.09	1.37	45.84	27
(0.5, 0.5)	1.63	1.91	16.78	17
(0.5, 1.0)	1.63	1.71	31.90	5
(0.5, 1.5)	1.09	1.48	42.13	36
(1.5, 0.5)	1.09	1.31	11.78	20
(1.5, 1.0)	1.09	1.23	22.64	13
(1.5, 1.5)	1.09	1.13	32.03	4

Table 9. Maximum spherical agility (normalized) for a six-wheel configuration with η_{opt}.

(F, G)	$\bar{\alpha}_{\max}$	$\mathcal{A}$	η_{opt} (deg)	Gain (%)
(1.0, 1.0)	2.67	2.67	35.26	–
(1.0, 0.5)	2.67	3.18	23.41	19
(1.0, 1.5)	1.78	2.25	46.02	26
(0.5, 0.5)	2.67	3.20	26.57	20
(0.5, 1.0)	2.67	2.67	35.26	–
(0.5, 1.5)	1.78	2.28	42.57	28
(1.5, 0.5)	1.78	2.24	14.48	26
(1.5, 1.0)	1.78	2.05	27.31	15
(1.5, 1.5)	1.78	1.83	37.76	3

Applying the agility envelope in practice

To illustrate the application of the agility envelope in a practical scenario, this section presents the simulation and analysis of the slew performance of a four reaction wheel spacecraft and highlights some of the tangible benefits that may be obtained by using the agility envelope for design in lieu of standard techniques.

Consider an example spacecraft with an inertia tensor given by

$$\mathbf{I} = \begin{bmatrix} 45.66 & 0.92 & 4.60 \\ 0.92 & 34.75 & -4.96 \\ 4.60 & -4.96 & 65.83 \end{bmatrix} \text{kg} \cdot \text{m}^2 \tag{57}$$

Converting to principal inertias, the inertia ratio tensor becomes

$$\mathbf{I} = 45.0 \text{ kg} \cdot \text{m}^2 \begin{bmatrix} 1 & 0 & 0 \\ 0 & 0.75 & 0 \\ 0 & 0 & 1.50 \end{bmatrix} \tag{58}$$

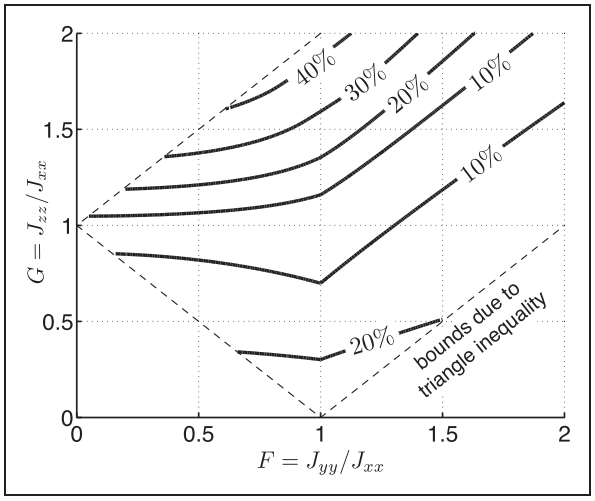

Figure 9. Percent increase in useable spherical acceleration for a NASA standard four-wheel configuration using the agility envelope.

with the first principal moment of inertia, $I_{xx} = 45.0\,\mathrm{kg}\cdot\mathrm{m}^2$ and $I_{\max} = 67.50\,\mathrm{kg}\cdot\mathrm{m}^2$. The inertia ratios are $F = 0.75$ and $G = 1.50$. All four wheels are assumed to be identical and to have a maximum torque capability of 0.2 Nm and a maximum slew momentum of 1.5 Nms for each wheel. The reaction wheel alignment is given in equation (38), however the angle η is not specified, but is rather taken as a design variable for optimization. The benefit of the agility envelope based design is illustrated by comparing the agility envelope optimized design against a standard design obtained by maximizing the spherical torque.

For the simulation, the spacecraft attitude kinematics are described using inertial quaternions of the form, $[q_1, q_2, q_3, q_4]$, with q_4 taken as the scalar term. The equation for the time derivative of the spacecraft attitude, with $\mathbf{q} = [q_1\ q_2\ q_3]^T$, is:

$$\dot{\mathbf{q}} = \frac{1}{2}(q_4^i\boldsymbol{\omega}^b - {}^i\boldsymbol{\omega}^b \times \mathbf{q}) \tag{59}$$

$$\dot{q}_4 = -\frac{1}{2}({}^i\boldsymbol{\omega}^b \cdot \mathbf{q}) \tag{60}$$

The vector ${}^i\boldsymbol{\omega}^b = [\omega_1\ \omega_2\ \omega_3]^T$ gives the angular rate of the spacecraft body reference frame b with respect to the inertial frame i.

The spacecraft dynamics, neglecting external disturbances, are given by

$${}^i\dot{\boldsymbol{\omega}}^b = \mathbf{I}^{-1}\left(-{}^i\boldsymbol{\omega}^b \times \left(\mathbf{I} + {}^i\boldsymbol{\omega}^b + \sum_{j=1}^{4}\mathbf{z}_j h_j\right) - \sum_{j=1}^{4}\mathbf{z}_j\tau_j\right) \tag{61}$$

where $\mathbf{I}$ is the spacecraft inertia tensor, $\mathbf{z}_j$ is a column vector from $\mathbf{Z} = [\mathbf{z_1}|\mathbf{z_2}|\mathbf{z_3}|\mathbf{z_4}]$, and τ_j is the torque produced by the jth reaction wheel. The momentum stored in the jth reaction wheel is h_j and the rate of change in this momentum is the control torque for that particular reaction wheel. Equations (59) to (61) are combined to give a set of first-order differential equations that describe the motion of the spacecraft in response to the reaction wheel torque commands.

To illustrate that it is indeed possible to achieve the performance enhancement that is possible by optimizing the skew angle η with the agility envelope, an attitude control simulation was performed using a quaternion error feedback control law[17] with rate and acceleration magnitude limits to implement a rest-to-rest slew of 90° about an arbitrary eigenaxis (since the acceleration and rate limits are spherical by design).

$$\tau^a = \mathbf{Z}^\dagger\tau^b_{\mathrm{cmd}} = \mathbf{Z}^\dagger\left(-K\mathbf{I}\mathbf{q}_e - C\mathbf{I}^i\boldsymbol{\omega}^b + {}^i\boldsymbol{\omega}^b \times \mathbf{I}^i\boldsymbol{\omega}^b\right) \tag{62}$$

where $\mathbf{q}_e$ is the quaternion error, K and C are properly defined feedback gains, and $\mathbf{Z}^\dagger$ denotes the pseudo-inverse control allocation to the individual reaction wheels.

The maximum spherical torque envelope (standard design) is obtained from the design charts by setting $\eta = 35.26°$ which yields $r_h = 1.63$ (Nms/Nms). This value for r_h is obtained from Table 6, equation (44) or Figure 7(b) with $F = G = 1$ and is the same as the value presented previously in Markley et al.[12]

Using the conventional design equation (4), the maximum slew rate is

$$\omega_{\max} = \frac{h_{\max}\, r_h}{I_{\max}} = 2.08\ \mathrm{deg/sec} \tag{63}$$

and the maximum acceleration is

$$\alpha_{\max} = \frac{\tau_{\max}\, r_h}{I_{\max}} = 0.28\ \mathrm{deg/sec}^2 \tag{64}$$

However, the skew angle may very well be different if the agility envelope is used to maximize the agility. For an agility envelope based design of the example spacecraft, the optimal skew angle is $\eta_{opt} = 43.85°$. This value of η is obtained from equation (43) or Figure 7(a), using the example inertia ratios. The predicted increase (32%) in performance can also be obtained from Figure 9. The radius of the normalized agility sphere is $\mathcal{A} = 1.44$, using (44). From the agility envelope design equations, then, the maximum slew rate is

$$\omega_{\max} = \frac{h_{\max}\, \mathcal{A}}{I_{xx}} = 2.75\ \mathrm{deg/sec} \tag{65}$$

and the maximum acceleration is

$$\alpha_{\max} = \frac{\tau_{\max}\, \mathcal{A}}{I_{xx}} = 0.38\ \mathrm{deg/sec}^2 \tag{66}$$

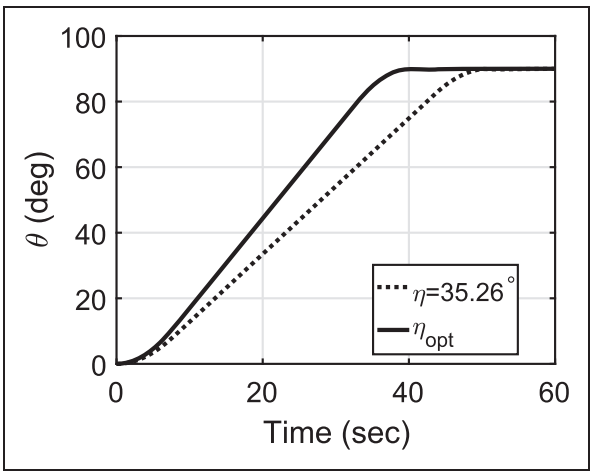

Figure 10. Time to complete a 90° eigenaxis rest-to-rest slew.

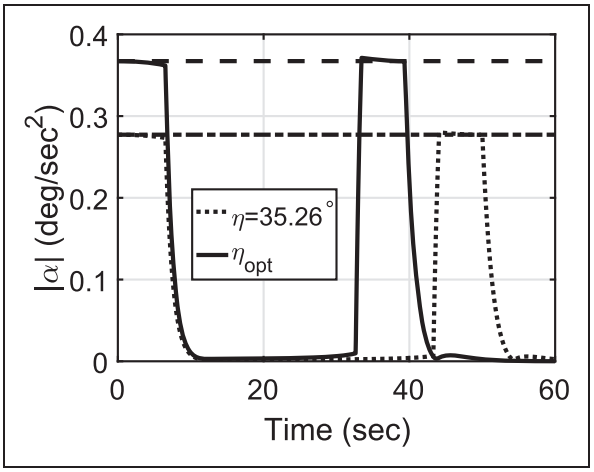

Figure 11. Body acceleration magnitude with respective limits shown.

Figures 10 to 12 show a simulation of the spacecraft executing the 90° rest-to-rest maneuver for both the standard and agility envelope-based designs. The dotted lines represent the performance achieved when the reaction wheels are configured to maximize the spherical torque envelope and the industry standard acceleration and rate limits (equations (63) and (64)) formulations. The solid lines show the performance using the optimized reaction wheel configuration obtained from the agility envelope to determine the maximum rate and acceleration limits. Figure 10 demonstrates how the agility envelope-based configuration completes the maneuver in less time than the standard one. The time to complete the maneuver corresponds closely with the analytical solution in (2).

Figure 11 shows that the implemented maneuver is a classical bang-off-bang maneuver, as expected, and that both systems operate at their respective limits for acceleration. Not shown, for brevity, is the rate profile which follows the trapezoid shape characteristic of a rate limited eigenaxis maneuver with the maximum rates being specified per equations (63) and (65), respectively.

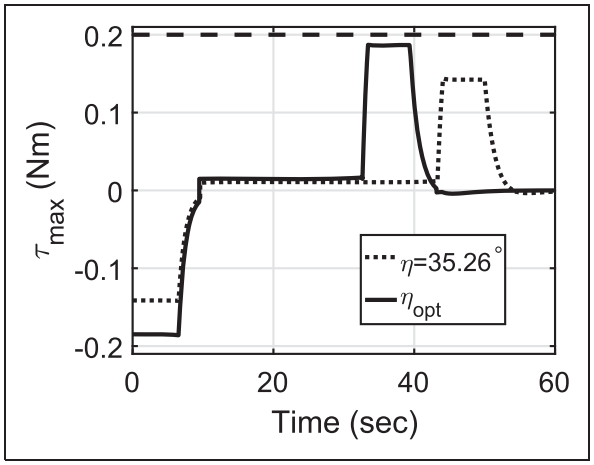

Figure 12. Comparison of maximum reaction wheel torque required by any wheel with reaction wheel limit shown as black dashed line.

The most important aspect of the simulation is seen in Figure 12 where the maximum torque of any given reaction wheel is plotted against time. The agility envelope based design allows for better utilization of the available reaction wheel torque because the commands are closer to the limiting values. This is the direct result of using the agility envelope to design the rate and acceleration limits as opposed to the standard method based on maximizing the spherical torque.

Conclusion

This paper presented a simple approach for constructing the agility envelope of a reaction wheel spacecraft. The key insight was the observation that the effect of the spacecraft inertia tensor is to rotate and scale the reaction wheel torque envelope through a series of affine transformations to give a new performance envelope described by the agility matrix, $\mathbf{A} = -\mathbf{I}^{-1}\mathbf{Z}$. The inscribed sphere of the new agility envelope provides a more accurate measure of the minimax slew capability of the satellite in comparison with the standard approach where the radius of the inscribed sphere of the torque envelope is divided by the maximum principal inertia. The conventional analysis can 'hide' the true capability of a reaction wheel attitude control system from the operator. The use of the agility envelope, on the other hand, allows the true minimax capability to be determined in order to reduce slew times without the need for larger, more costly hardware or the implementation of new control algorithms. This aspect was demonstrated via the simulation of a four reaction wheel attitude control system. The agility envelope can also be used in the design phase of a spacecraft to adjust the reaction wheel skew angle to reduce requirements on the wheels. This reduces size, weight, and power

requirements and ultimately the cost of the attitude control system. To facilitate design analysis and trade studies, simple expressions and design curves were developed for defining the minimax agility (both angular acceleration and rate) in terms of inertia ratios and the ideal skew angle. These results show that the skew angle that maximizes agility is generally not the same as the skew angle that maximizes the spherical torque/momentum envelope.

Declaration of Conflicting Interests

The author(s) declared no potential conflicts of interest with respect to the research, authorship, and/or publication of this article.

Funding

The author(s) received no financial support for the research, authorship, and/or publication of this article.

ORCID iD

Jeffery T King http://orcid.org/0000-0003-3539-4997

References

1. Karpenko M, Bhatt S, Bedrossian N, et al. Flight implementation of shortest-time maneuvers for imaging satellites. *J Guid Control Dyn* 2014; 37: 1069–1079.
2. Sidi MJ. *Spacecraft dynamics and control: A practical engineering approach*. New York: Cambridge University Press, 2000. ISBN 9780521787802.
3. Hablani HB. Target acquisition, tracking, spacecraft attitude control, and vibration suppression with IPFM reaction jet controllers. In: *Proceedings of the AIAA guidance, navigation, and control conference*, Hilton Head, SC, August 1992.
4. Creamer G, DeLaHunt P, Gates S, et al. Attitude determination and control of clementine during lunar mapping. *J Guid Control Dyn* 1996; 19: 505–511.
5. Sedalk JE and Houghton MB. Lunar reconnaissance orbiter (LRO) attitude maneuver planning. In: *International symposium on spaceflight dynamics*, Toulouse, France, September 2009.
6. Karpenko M, King J and Ross IM. Agilitoid-based design analysis of next generation attitude control systems. In: *38th annual AAS guidance & control conference*, Breckenridge, CO, January 2015. Paper number: AAS 15-047.
7. King J and Karpenko M. A simple approach for predicting time-optimal slew capability. *Acta Astronaut* 2016; 120: 159–170.
8. Kaplan MH. *Modern spacecraft dynamics and control*. New York: John Wiley & Sons, 1976.
9. Fleming A, Sekhavat P and Ross IM. Minimum-time reorientation of a rigid body. *J Guid Control Dyn* 2010; 33: 160–170.
10. King JT and Karpenko M. Estimation of optimal control benefits using the agilitoid concept. In: *25th AAS/AIAA space flight mechanics meeting*, Williamsburg, VA, January 2015. Paper number: AAS 15-380.
11. Hablani H. Sun-tracking commands and reaction wheel sizing with configuration optimization. *J Guid Control Dyn* 1994; 17: 805–814.
12. Markley FL, Reynolds RG, Liu FX, et al. Maximum torque and momentum envelopes for reaction wheel arrays. *J Guid Control Dyn* 2010; 33: 1606–1614.
13. Markley FL and Crassidis JL. *Fundamental of spacecraft attitude determination and control*. New York: Springer-Verlag, 2014.
14. Larson WJ and Wertz JR (eds) *Space mission analysis and design*. 2nd ed. Torrance, CA: Microcosm, Inc, 1992. ISBN 0792319982.
15. Rockafellar RT. *Convex analysis*. Princeton, NJ: Princeton University Press, 1997.
16. Barvinok AI. *A course in convexity, graduate studies in mathematics*. vol. 54. Providence, RI: American Mathematical Society, 2002.
17. Wie B. *Space vehicle dynamics and control*. Reston, VA: AIAA, 2008. ISBN 9781615830442.